Atomic Force Microscopy

Sam Lucas

May 3, 2017

Partners with Mitch Mezeivtch

Phys 457W Experimental Physics – Spring 2017

Prof. J. Shan

Abstract:

In this paper, for the purpose of better understanding the mechanisms, capabilities, and shortcomings of atomic force microscopy, we investigate the high resolution scans of a Nanosurf easyScan2 atomic force microscope. The primary samples used for analysis were a basic calibration grid as well as molybdenum disulfide crystals grown on a silicon substrate. Prominently formed crystals were located on the substrate, captured in scans and, along with scans of the calibration grid, were exported as raw topographical data. This data was then parsed in MATLAB in order to make precise measurements and generate comprehensive surface plots. The width of the steps on our calibration grid were found to be 3.685 ± 0.566 μm and the height was found to be 29.43 ± 8.77 nm. Both of these measurements fall in line with expected values, which are about 4 μm for width and about 25 nm for height. The first of two successfully identified crystals on our sample had edges measuring 1.264 ± 0.566 μm and a height of 10.08 ± 8.77 nm. The edges of the second crystal measured 3.772 ± 0.566 μm and the height was found to be 11.99 ± 8.77 nm. It was determined that the uncertainty of the z-axis measurements is far greater than is necessary to precisely measure individual steps of a MoS_2 crystal.

I. Introduction

In this experiment we sought to demonstrate and evaluate the potential of atomic force microscopy (AFM). AFM is a subset of scanning probe microscopy which is the practice of forming images of surfaces using a physical probe to scan the specimen. It is also the successor to scanning tunneling microscopy which utilizes a scan head with a conductive tip and applies a tunneling current when brought very near to a conductive specimen. This current can be used to control the tip-surface distance very precisely and can be measured in order to produce images with enormous resolution. The primary drawback of this method is its restriction to conductive surfaces, which is where AFM comes in. An AFM probe is capable of scanning insulating surfaces because it does not rely on a tunneling current. Instead, the tip is brought near enough to the surface to allow for atomic-range forces to act between the tip and surface. The force acting on the tip as it scans, which is determined by the deflection of the cantilever, is then processed into a detailed map of the surface.[1 2]

Our goal was firstly to identify the overall accuracy of our easyScan2 atomic force microscope by scanning a calibration grid comprised of square steps with a known height and width. The results of these scans would then determine whether the microscope had the necessary precision to measure more discrete structures such as the MoS_2 crystals. These crystals are often quite small, possessing an equilateral triangular formation with a side length no greater than 305 μm under ideal conditions, and more commonly a fraction of that size in less than ideal conditions.[3] Moreover, the step height of these crystals is an even more discrete quantity, with individual layers measuring 0.6-0.7 nm on average.

Our second goal was to examine the effect of the scan resolution on the quality of the data. A logical conjecture might assert that a higher resolution scan is wholly proportional to a higher quality image. However, such a conjecture would operate under the assumption of an ideal scanning device. The quality of the scan, down to each individual data point, is reliant on the stability of the scanner and its environment. Although most measures were taken to minimize the impact of these factors on scan quality they could not be entirely eliminated under our lab conditions and with our quality of equipment. As such, there would be some small chance of an erroneous measurement for every point of data collected, and so it would follow that the greater amount of data collected the greater the odds of finding artifacts in the data. We sought to determine to what extent this would affect the quality of our results.

Assuming the scanner was sufficiently capable of measuring discrete features, and with relatively low artifact production, our final goal was to locate and capture high resolution scans of well-defined MoS_2 crystals. The samples which were examined had been prepared by a third party, presumably via chemical vapor deposition (CVD) with solid molybdenum trioxide and sulfur precursors.[4] CVD is the chemical process by which a substrate, in this case silicon, is exposed to volatile precursors which react on the surface in order to produce the desired deposit.[5] If the precision of the scanner allowed for it, we aimed to pinpoint roughly how many layers were present on each of the successfully captured crystals.

II. Theory

An AFM probe consists of a cantilever with a small tip at the end. The primary physical mechanism acting upon the tip which is utilized for precise measurement is the Lennard-Jones potential. The potential energy resulting from the interaction between two non-bonding atoms or molecules based on their distance of separation is described by this mathematical model. The general trend of intermolecular potential as a function of distance between molecules r(σ) is modeled in Figure 1 below.[6]

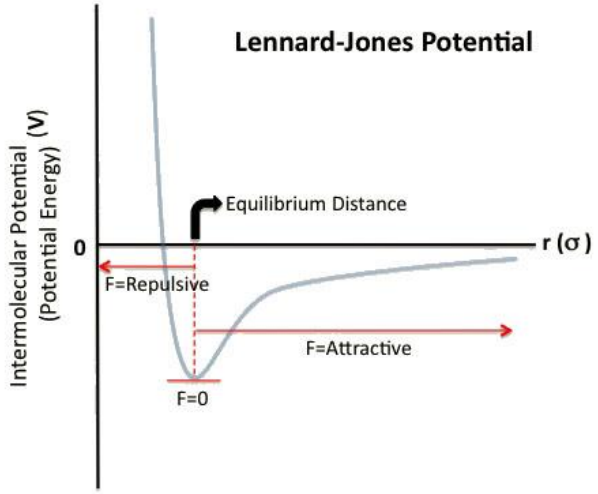

Figure 1 - Intermolecular potential energy as a function of distance between molecules

The steep repulsive curve which influences the molecules at very near distances is the result of the atoms becoming close enough for their electron clouds to repel one another. The attractive forces which influence the molecules at distances greater than that of the potential minimum are the result of Van der Waals forces or, more particularly, London dispersion forces. The displacement of electrons in each molecule causes a momentary polarization which allows for an attractive force.[7]

The cantilever on our scan head is made to vibrate at fixed amplitudes and at a frequency very near to its resonance. The repulsive forces acting on the tip as it is drawn near to the specimen will increase the resonance frequency and consequently dampen the vibrational amplitude. The opposite effect is seen as the tip distances itself from the surface. The resulting fluctuations in vibrational amplitude are monitored by a laser which is focused on the tip. Information from the laser is then reflected onto a photodiode detector and subsequently processed into a highly detailed image. The information from the laser is also utilized to manage the distance between the tip and the surface which is adjusted with precise piezoelectric motors so as the avoid direct contact with the surface which could potential damage the tip and disrupt data collection.

III. Materials and Methods

For each step of our experiment we utilized an easyScan2 atomic force microscope system, depicted in Figure 2 below. The primary components of the system include the scan head which contains the cantilever holding the scanning tip and is situated on a base acting as the sample stage. The base is equipped with shock-resistant legs to minimize vibrations from the environment which might contribute to background noise in frequency readings or artifacts in scans. The scan head is attached to the easyScan2 controller which is in turn connected to a computer using the specialized easyScan2 software, wherein the images and topographical data is generated. This data was then exported to MATLAB where we were able to use custom code to generate comprehensive surface plots and take precise measurements in all three dimensions.

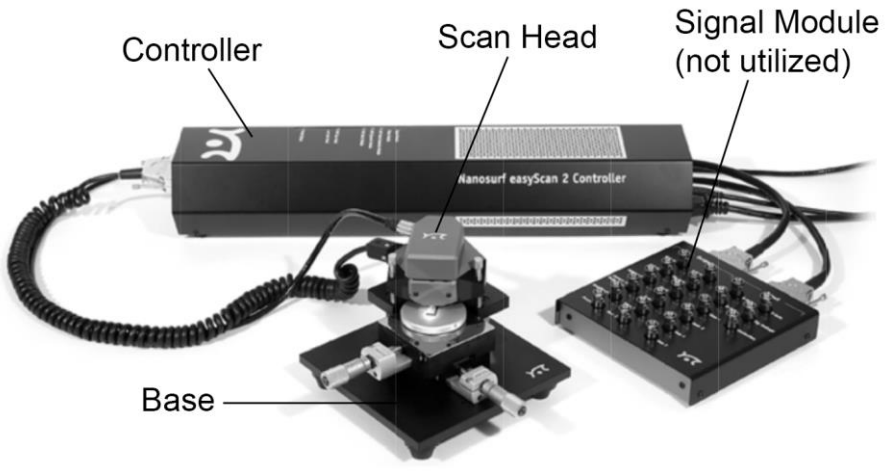

Figure 2 - easyScan2 atomic force microscope system [8]

The procedure for capturing the calibration grid was straightforward and simply involved positioning and scanning the sample. However, the general procedure for scanning the MoS_2 crystals was slightly more complicated. In an effort to locate these small triangular crystals on the sample we had to first run scans over a larger surface area and at a lower resolution, for the sake of using our time efficiently. Once a structure was spotted which resembled a crystal we then zoomed in on the area and proceeded to take a higher resolution scan. Often the structure would be a false positive and would more than likely be some residual sulfur left over from the CVD. However, if a crystal was successfully identified then the post-scan data would be ready to export and measure.

IV. Results, Analysis and Data

For the first step of our experiment we found the step height of the calibration grid to be 29.43 ± 8.77 nm and the step width to be 3.685 ± 0.566 μm. These both fell in line with the rough expected values of 25 nm and 4 μm respectively, albeit with rather large error. The quality of the scan, in the interest of time, was not at the maximum resolution possible for our system. The resolution used for this scan was 256 points per line (ppl) which, when scanning over a 50 μm^2 surface as was done for the calibration grid, leaves an inherent minimum uncertainty of ±0.195 μm for x- and y-axis data. The additional uncertainty found in the scan can be attributed to a less than optimal scanner tip stability which led to a somewhat rougher graph than would be considered ideal. As for the error on the z-axis, the error can be attributed to a sub-optimal z-axis calibration. The calibration is done both manually and digitally prior to running any scans, but is very difficult to perfect. The calibration in addition to the same drawbacks from tip instability are likely the primary contributors to the error bar on the z-axis. It should be noted that in the calculation of z-axis uncertainty there was an exclusion of outlier data points that were reasonably determined to be artifacts of a scan with imperfect stability.

Depicted in Figure 3 below are two surface plots generated from the scans of our calibration grid, the first being the scan which was used to determine uncertainty in the first step of our experiment, the second being a lower resolution scan at 128 ppl. An example of the z-axis and frequency amplitude images generated directly in our easyScan2 software can be seen in Figure 6 of the appendix. The drastic increase in the number of artifacts for the higher resolution scan is plainly visible upon comparison. Upon counting the number of outlier data points beyond the uncertainty of the step height in MATLAB we found that the scan with the higher resolution saw a 133.33% increase in production of artifacts compared to the lower resolution scan. Since the resolution of the left plot is double that of the right, this is 33.33% more artifact production than would be expected from a linear relation between resolution and artifact production. That said, this is not a significant enough difference to assert the relationship is not necessarily roughly linear, as it is only two data points. In addition, these two scans were taken on two separate days which required a recalibration of the z-axis in between the two scans, and may have even involved a change in scanner tip as well. As such, the quantitative findings of this resolution comparison are not substantial enough to be conclusive.

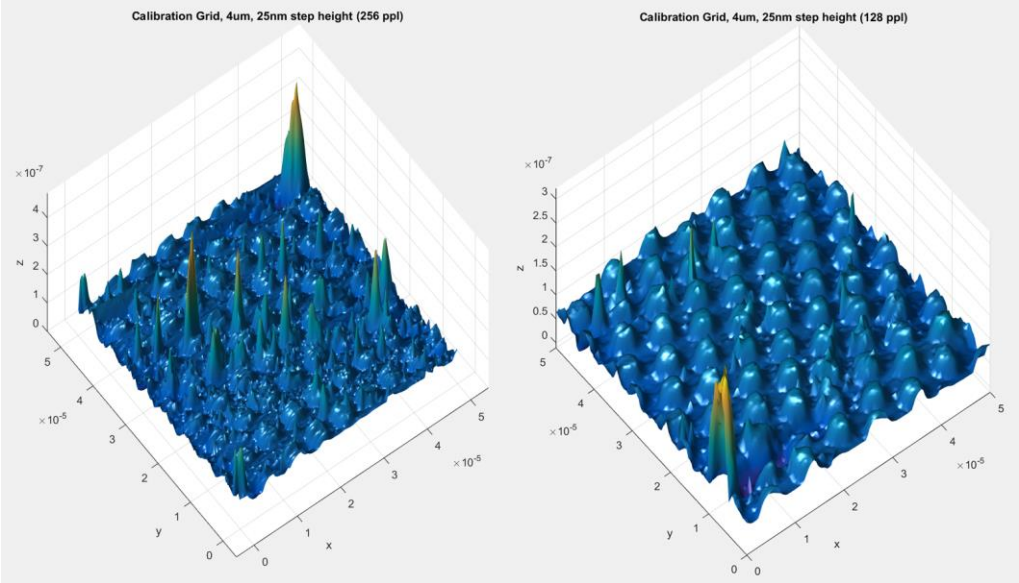

Figure 3 - Surface plot of scan data for calibration grid in 256 ppl (left) and 128 ppl (right)

Lastly, in the search for well-defined MoS_2 crystals we successfully located two structures which were scanned and exported into the surface plots depicted in Figures 4 and 5 below. An example of the z-axis and frequency amplitude data generated in the easyScan2 software directly for the first of these two crystals can be seen in Figure 7 of the appendix. The first crystal to be successfully found, seen in Figure 4, was found to have a height of 10.08 ± 8.77 nm and edges measuring 1.264 ± 0.566 µm. It is worth noting that the uncertainty from the scan itself was smaller than this figure but was increased upon factoring in the uncertainty of the calibration grid which had known values to compare with. Also note the large spike around the center of the crystal, denoted with a red arrow, which can be reasonably asserted is the site of the seed from which the crystal grew outward, as it is comprised of too many data points to be dismissed as an artifact.

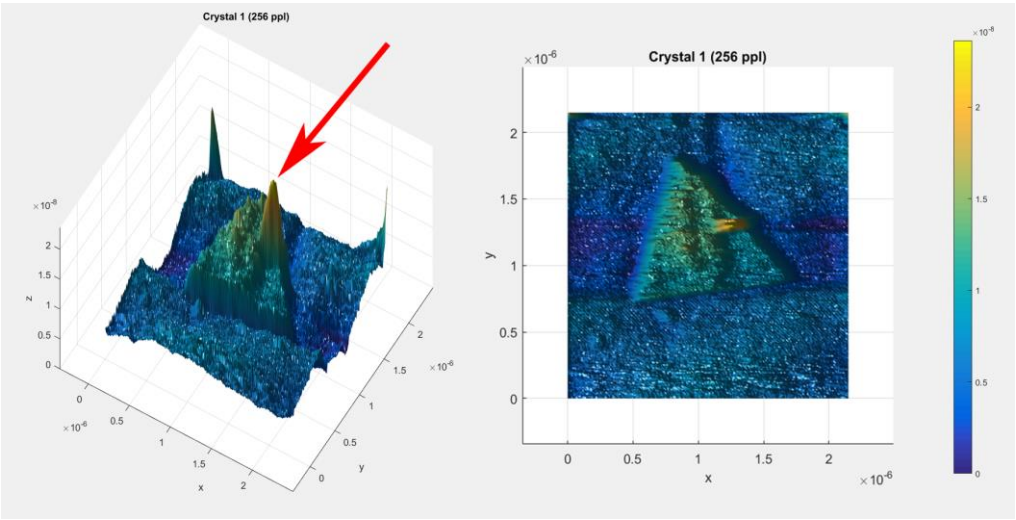

Figure 4 - First successfully identified MoS_2 crystal, isometric view (left) and top view (right), seed marked with red arrow

The second successfully identified crystal is depicted in Figure 5 below. This crystal was overlapping with another, slightly less prominent crystal which extends out of the range of the scan area, but the measurements were preformed solely on the crystal which is present in its entirety. The height of this crystal was found to be 11.99 ± 8.77 nm and the edges were measured at 3.772 ± 0.566 µm. The same logic was applied to the decided uncertainty as the first crystal, as this scan also had an inherent uncertainty which was less than that of the calibration scans. As this crystal is overlapping with another we can see two prominent spikes for each of the two seeds they originated from, each denoted with a red arrow. As the uncertainty for z-axis data is far greater than the height of an individual MoS_2 crystal step we cannot confidently identify a number of layers on either of the two successfully identified crystals.

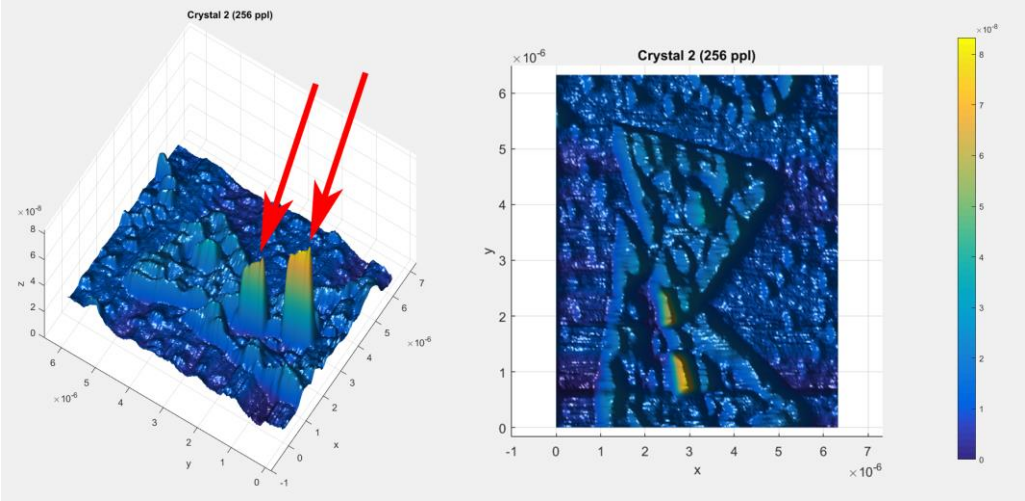

Figure 5 - Second successfully identified MoS_2 crystal, isometric view (left) and top view (right), seeds marked with red arrow

V. Conclusion

Had the resolution of our scans been set higher, our atomic force microscope had the potential to produce incredibly precise x- and y-axis data. The z-axis, on the other hand, was very difficult to calibrate for a precision of data much greater than what we were able to achieve. As such, the precision of our instrument was decidedly too poor to measure individual layers of a MoS_2 crystal. Additionally, the stability of our scanner tip was brought into question by the comparison of different resolution scans for our calibration grid, as well as by the general coarseness of our crystal scans. The repeated replacement of the scanner tip as well as the consistent recalibration of the z-axis were both likely major contributors to the error in our topological data. The production of artifacts was certainly increased in higher resolution scans, as predicted, but there was not strong enough quantitative data to assert whether or not this relationship deviated from the expected linear correlation.

VI. References

1. N.a (n.d.). AFM+STM Manual_2015.pdf | Powered By Box. *Psu.app.box.com*. Retrieved from https://psu.app.box.com/v/phys559-afmstm

2. N.a (6 Apr. 2005.). Fundamental Theory of Atomic Force Microscopy. *Nanoscience.gatech.edu*. Retrieved from http://www.nanoscience.gatech.edu/zlwang/research/afm.html

3. Chen, Jianyi (1 Apr. 2016.). Chemical Vapor Deposition of High-Quality Large-Sized MoS2 Crystals on Silicon Dioxide Substrates. *Onlinelibrary.wiley.com*. Retrieved from http://onlinelibrary.wiley.com/doi/10.1002/advs.201600033/full

4. Arend M. Van Der Zande (5 May 2013.). Grains and grain boundaries in highly crystalline monolayer molybdenum disulphide : Nature Materials : Nature Research. *Nature.com*. Retrieved from https://www.nature.com/nmat/journal/v12/n6/full/nmat3633.html

5. Wikipedia Contributors (30 Apr. 2017.). Chemical vapor deposition. *Wikipedia, the Free Encyclopedia*. Retrieved from https://en.wikipedia.org/wiki/Chemical_vapor_deposition

6. Chemistry LibreTexts (2 Oct. 2013.). Lennard-Jones Potential. *Chemistry LibreTexts*. Retrieved from https://chem.libretexts.org/Core/Physical_and_Theoretical_Chemistry/Physical_Properties_of_Matter/Atomic_and_Molecular_Properties/Intermolecular_Forces/Specific_Interactions/Lennard-Jones_Potential

7. Chemistry LibreTexts (2 Oct. 2013.). Van der Waals Forces. *Chemistry LibreTexts*. Retrieved from https://chem.libretexts.org/Core/Physical_and_Theoretical_Chemistry/Physical_Properties_of_Matter/Atomic_and_Molecular_Properties/Intermolecular_Forces/Van_der_Waals_Forces

8. N.a (6 Jul. 2006.). . *Virlab.virginia.edu*. Retrieved from http://virlab.virginia.edu/Nanoscience_class/labs/materials/easyScan%202%20-%20AFM%20Manual.pdf

VII. Appendix

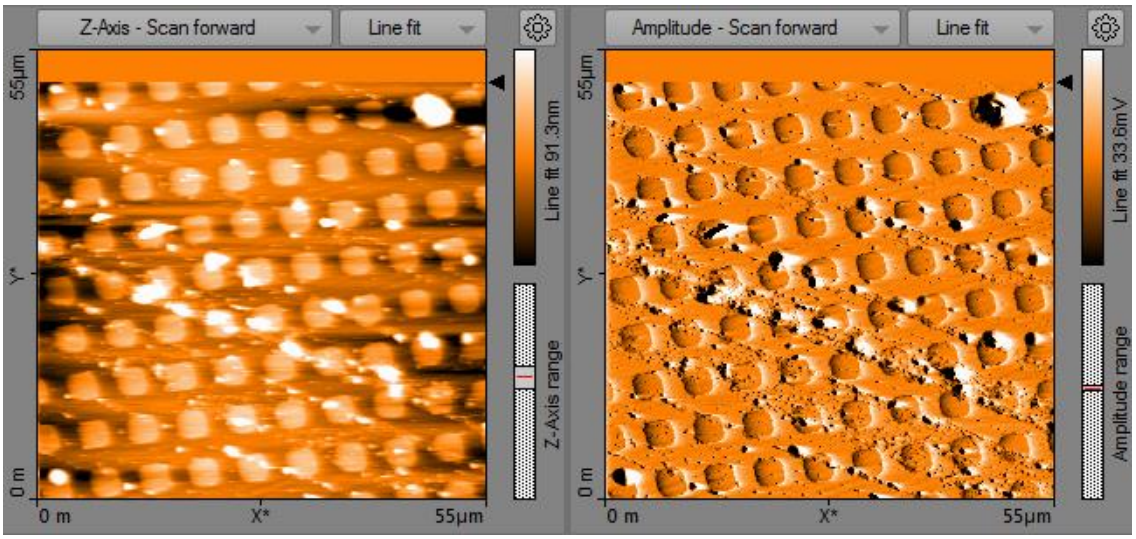

Figure 6 - Example of data generated in easyScan2 software, z-axis data (left) and frequency amplitude data (right)

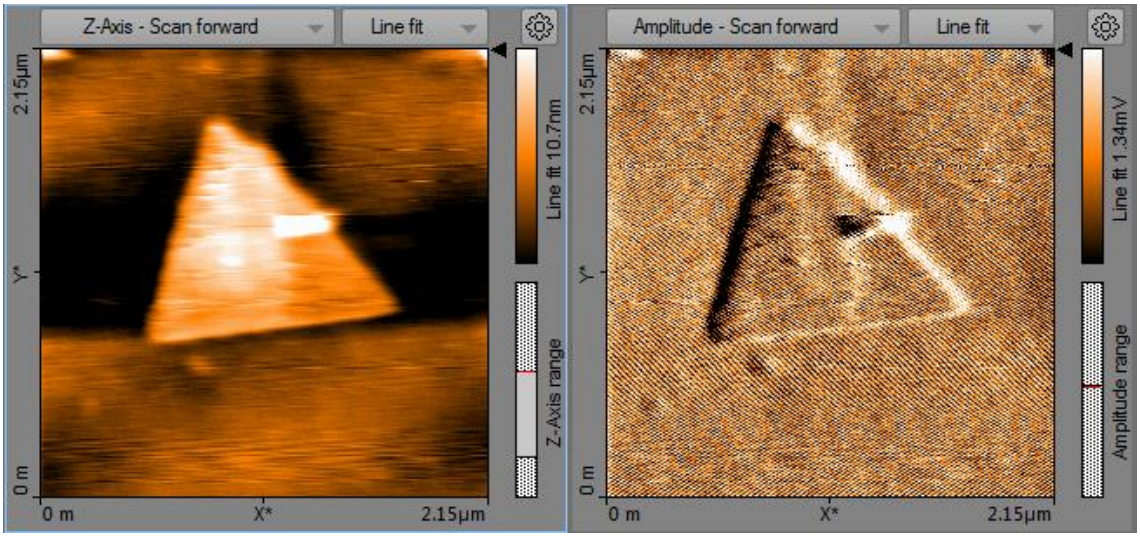

Figure 7 - Example of data generated in easyScan2 software, z-axis data (left) and frequency amplitude data (right)